Mathematical Modelling of Membrane CO_2 Capture for Blue Hydrogen Production

Boram Gu *

* *School of Chemical Engineering, Chonnam National University, Gwangju, Republic of Korea (e-mail: boram.gu@jnu.ac.kr).*

Abstract: Membrane gas separation is a promising technology for carbon capture due to its high energy efficiency, easy scale-up and simple operation. In particular, carbon capture followed by syngas production becomes important as hydrogen is deemed to be a prominent candidate to substitute fossil fuels. Therefore there is the need of understanding the effects of process operation and design variables on hydrogen production and CO_2 separation efficiency in membrane gas capture for blue hydrogen production. This work presents a predictive model for a hollow fibre membrane module that can be applied to multicomponent gas separation. The developed model accounts for concentration polarisation in a multicomponent system, caused by limited mass transfer near selective membrane barriers, as well as axial variations in gas flowrates and pressures. A number of simulations are undertaken by varying membrane module properties and feed flowrates in order to investigate their effects on product quantity and quality. Finally the model is validated against experimental data available in the literature.

Keywords: CO_2 capture, blue hydrogen production, membrane gas separation, hollow fibre modules, mathematical modelling

1. INTRODUCTION

Carbon capture technologies have attracted immense attention worldwide as an attempt to reduce an environmental impact in energy and chemical industries as well as means to separate impurities from a gas mixture as in natural gas processing (Siagian et al., 2019). In particular, integrating carbon dioxide (CO_2) capture with hydrogen (H_2) production has been of interest for the production of environmental-friendly blue H_2 from the current fossil fuel-based H_2 production processes, as H_2 has become an important energy source to replace fossil fuels in the transport and industrial sectors (Voldsund et al., 2016; Antonini et al., 2020). CO_2 can be captured by various methods: chemical absorption, adsorption and membrane separation (Zhang et al., 2020). Among them, amine-based absorption has been most widely implemented due to its high separation efficiency, high capacity and capability of processing a gas stream with low CO_2 loading (Siagian et al., 2019; Wang et al., 2011; Xu et al., 2019). Despite technological improvement, there are several drawbacks such as high energy requirement for solvent regeneration, equipment problems accompanied by the use of amines, operational difficulties in packed columns such as flooding and entrainment (Siagian et al., 2019; Wang et al., 2011; Xu et al., 2019). Membrane-based gas separation has been thought of as an alternative, where a partial pressure difference between two gas streams separated by a selective membrane is the main driving force for gas separation. It is thought to be advantageous over conventional chemical absorption in terms of energy efficiency, modularity and operational simplicity (Siagian et al., 2019; Xu et al., 2019).

Many researchers have attempted to develop high selectivity and high flux membranes that can be applied to a wide range of temperatures and pressures using different materials (Voldsund et al., 2016; Adhikari and Fernando, 2006; Ockwig and Nenoff, 2007; Khalilpour et al., 2015; Scholes et al., 2010; Lu et al., 2007). Gas permeance for each gas species is the key parameter that determines product gas quality and quantity. Also the extent of mass transfer within a membrane module affects the concentration of gas species at membrane surfaces, which is different from its bulk value due to selective gas permeation and limited mass transfer. Since membrane technologies for gas separation are still under development, especially for CO_2 capture and H_2 purification, a reliable mathematical model for membrane CO_2 capture with experimental validation can be useful in elucidating the intricate relationships between process variables and performance indicators.

There are a number of modelling studies for membrane gas separation (Feng et al., 1999; Chu et al., 2019; Gilassi et al., 2018). Chu et al. (2019) developed a mathematical model of hollow fibre membrane modules for CO_2 removal from natural gas consisting of five types of hydrocarbons. Although their model is capable of dealing with a multicomponent system with various flow configurations, concentration polarisation caused by different permeability of each gas component has not been taken into account, which could influence the overall separation performance depending on the module design and operating conditions. Several studies presented theoretical strategies to account for concentration polarisation (He et al., 1999; Wang et al., 2002; Nagy et al., 2013). However, the derived concentration polarisation formulas can only be applied to a binary

system or were not coupled with a predictive model of membrane modules.

In this study, a mathematical model of hollow fibre membrane modules is developed for multicomponent gas separation, followed by fossil fuel-based H_2 production. The developed model is capable of predicting gas concentrations at membrane surfaces via the multicomponent concentration polarisation model as well as axial variations in flowrates, concentrations and pressures for various flow configurations. A parametric study is undertaken by varying gas permeances, selectivities and mass transfer coefficient in order to quantitatively assess their effects on product gas purities and stage cuts. It is believed that the predictive model can be used to provide an insight into process design and optimisation towards improved process performance depending on different membrane materials and modules.

2. MODELLING METHODS

2.1 Process Overview

The overview of hollow fibre membrane CO_2 capture followed by fossil fuel-based H_2 production is shown in Fig 1. As a result of steam methane reforming and water gas shift reactions, H_2 and CO_2 are mainly obtained at 70-80 mol% and 15-25 mol%, respectively, with a small amount of unconverted CO and CH_4 (Voldsund et al., 2016). The shifted syngas mixture is fed to hollow fibre membrane modules for separation. Membranes can be either H_2 selective or CO_2 selective. When an H_2 selective membrane is used, high purity of H_2 is achieved in a permeate stream. On the other hand, using a CO_2 selective membrane leads to a CO_2 rich permeate and concentrated H_2 in a retentate stream. As depicted in Fig 1b, feed and permeate streams can flow either inside the fibres or the module, i.e., feed in the tube or in the shell. Also the direction of two flows can be either co-current or counter-current. Sweep gas can optionally be introduced in order to maximise productivity. Concentration polarisation resulting from selective gas permeation and limited mass transfer is illustrated in Fig 1c. The most permeable component becomes depleted near the membrane walls due to its high permeation rate, while the fractions of other components become relatively be elevated. The concentration polarisation phenomena are known to be the common performance inhibitor in many membrane processes. Polarised concentrations of each component should be taken into consideration for an accurate calculation of permeation fluxes.

2.2 Modelling Hollow Fibre Membrane Gas Separation

A one-dimensional (1D) steady-state mathematical model of hollow fibre membranes for gas separation is developed by assuming a negligible portion of transverse flow near the inlet and outlet of shell-side flow, as can be seen in Fig 1b. The developed model mainly consists of three elements: gas permeation, concentration polarisation and axial variations of molar flowrates and pressures. Feed gas is simplified to contain four components, H_2, CO_2, CH_4 and CO. It is assumed that sweep gas is not used; the model can easily be adapted to include sweep gas via applying relevant boundary conditions. Temperature

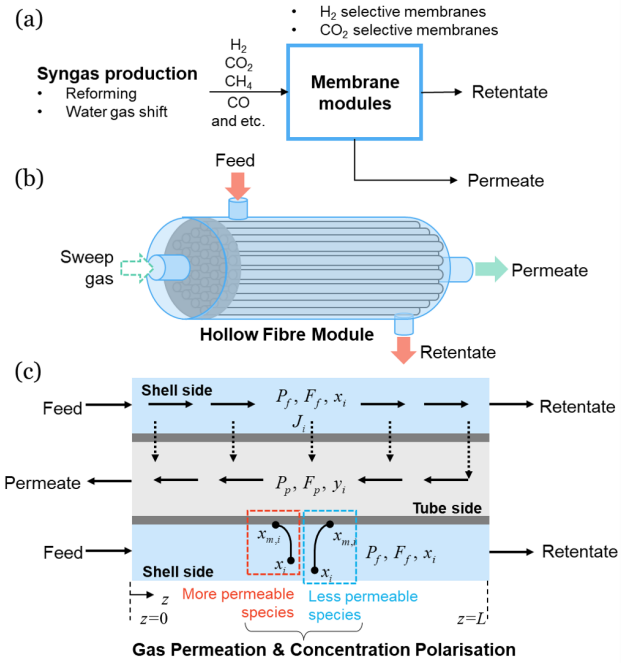

Fig. 1. The overview of membrane CO_2 capture for H_2 production. (a) A simplified process diagram, (b) a hollow fibre membrane module and (c) mass transfer phenomena within the membrane module.

variations are neglected here under the assumption of isothermal operation. Finally the ideal gas behaviour is assumed for simplicity.

Gas Permeation Fluxes Permeate fluxes are governed by partial pressure differences between the feed and permeate streams.

$$J_i = a_i \left(P_f x_{m,i} - P_p y_i\right) \text{ for } i = 1 \text{ to } n \tag{1}$$

where J is the permeation flux in mol/(m^2·s), a the permeance in mol/(m^2·s·Pa), P the pressure, x the molar fraction in the feed stream and y the molar fraction in the permeate stream. The subscripts i, m, f and p denote i-component, membrane, feed and permeate, respectively.

Concentration Polarisation A model for concentration polarisation is derived using volumetric fluxes for 1- to n-component, as shown in Eqs (2) and (3).

$$N_i = A_i \left(P_f x_{m,i} - P_p y_i\right) \text{ for } i = 1 \text{ to } (n-1) \tag{2}$$

$$N_n = A_n \left[P_f \left(1 - \sum_i^{n-1} x_{m,i}\right) - P_p \left(1 - \sum_i^{n-1} y_i\right)\right] \tag{3}$$

where N is the volumetric flux m^3/(m^2·s) and A the permeance parameter in the unit of m^3/(m^2·s·Pa), which can be calculated by $A_i = a_i M_{w,i}/\rho_i$ where M_w is the molecular weight and ρ the density. Also the volumetric fluxes in the boundary layer near the membrane surfaces at each local differential membrane area can be expressed as a function of local bulk concentration x and membrane wall concentration x_m.

$$N_i = k \left(x_i - x_{m,i}\right) X + x_i N_T \text{ for } i = 1 \text{ to } (n-1) \tag{4}$$

$$N_n = -k\left(\sum_i^{n-1} x_i - \sum_i^{n-1} x_{m,i}\right) X + \left(1 - \sum_i^{n-1} x_i\right) N_T \quad (5)$$
$$\text{where } X = \frac{P_f}{P_{ref}} \frac{T_{ref}}{T}$$

where k is the mass transfer coefficient in m/s and N_T the total volumetric flux. T_{ref} and P_{ref} are the reference temperature (273.15 K) and pressure (1 atm), respectively. The total volumetric flux can be calculated by summing Eqs (2) and (3) for all components and is expressed as follows:

$$N_T = P_f \left[\sum_i^{n-1} A_i x_{m,i} - A_n \sum_i^{n-1} x_{m,i}\right] + Y$$
$$\text{where } Y = A_n (P_f - P_p) - P_p \left[\sum_i^{n-1} A_i y_i - A_n \sum_n^{n-1} y_i\right] \quad (6)$$

By substituting Eq (6) into Eq (4) and equating Eqs (2) and (4), a total of $(n-1)$ equations can be constructed:

$$x_{m,i}\left(A_i P_f + kX - x_i P_f \Delta A_i\right) - x_i P_f \sum_{j \neq i}^{n-1} \Delta A_j x_{m,j}$$
$$= A_i P_p y_i + kX x_i + x_i Y \text{ for } i = 1 \text{ to } (n-1)$$
$$\text{where } \Delta A = A - A_n \quad (7)$$

Therefore the array of polarised concentrations of 1- to $(n-1)$-component, $\mathbf{x_m}$, can be obtained via Eqs (8) to (10).

$$\mathbf{x_m} = \mathbf{M}^{-1}\mathbf{b} \quad (8)$$

$$m_{ij} = \begin{cases} A_i P_f + kX - x_i P_f \Delta A_i \text{ for } j = i \\ -x_j P_f \Delta A_i \text{ for } j \neq i \end{cases} \quad (9)$$

$$b_i = A_i P_p y_i + kX x_i + x_i Y \text{ for } i = 1 \text{ to } (n-1) \quad (10)$$

The mole fraction of the final component, $x_{m,n}$, is calculated using the follwoing relationship.

$$x_{m,n} = 1 - \sum_i^{n-1} x_{m,i} \quad (11)$$

Component Balances Molar flowrates of each component in the feed and permeate sides are resolved by the component balances. Based on Fig 1c, a feed gas flows from $z = 0$ to L, which is the length of fibres.

$$\frac{dF_{f,i}}{dz} = -J_i \pi D_o N_f \quad (12)$$

$$\frac{dF_{p,i}}{dz} = \pm J_i \pi D_o N_f \quad (13)$$

where F is the molar flowrate in mol/s, D_o the outer fibre diameter and N_f the number of fibres. Depending on the flow direction, i.e., co-current or counter-current flows, the sign of the right-hand side term in Eq (13) is determined. Using the molar flowrates resolved by the set of ordinary differential equations, each molar fraction is calculated and used to calculate polarised concentrations and permeate fluxes as mentioned above. In addition, axial pressure variations are taken into account via the Hagen-Poiseuille equation, which can be found in the literature (Chu et al., 2019).

Boundary Conditions The model equations in Eqs (12) and (13) are solved by applying the following boundary conditions.

$$F_{f,i}|_{z=0} = x_{i,0} F_{f,0} \quad (14)$$

$$\left.\frac{dF_{p,i}}{dz}\right|_{z=0} = J_i|_{z=0} \pi D_o N_f \text{ for co-current flow} \quad (15)$$

$$F_{p,i}|_{z=0} = \int_{z=0}^{z=L} J_i \pi D_o N_f dz \text{ for counter-current flow} \quad (16)$$

For the pressure equations, operating pressure at the entrance of the feed channel is applied while the atmospheric pressure (1×10^5 Pa) is imposed at the exit of the permeate channel.

2.3 Solution Procedure and Simulation Conditions

The differential model equations and boundary conditions and integral boundary conditions in Eqs (12) to (16) are converted to algebraic equations via the first order backward finite difference method. An iterative procedure is employed to apply the boundary conditions for the permeate molar flowrates, i.e., the fixed point iteration for the co-current flow and the shooting method for the counter-current flow. The model equations and numerical procedures are implemented in MATLAB.

Model parameters, membrane module specifications and feed conditions used for simulations are listed in Table 1. An H_2 selective membrane is assumed for a representative case with its permeance and H_2/CO_2 and H_2/CH_4 selectivities reported in Adhikari and Fernando (2006), while H_2/CO is chosen based on Lu et al. (2007). The mass transfer coefficient is assumed to be constant throughout the membrane module (Nagy et al., 2013) for simplicity, although a mass transfer coefficient might vary depending on hydrodynamics and module designs. Module specifications are found in Chu et al. (2019). Feed conditions are chosen to be within a reported range (Voldsund et al., 2016). For a parametric study, H_2 permeance (or CO_2 permeance), H_2/CO_2 (or CO_2/H_2) selectivity and mass transfer coefficient are varied, whose values are addressed later.

Table 1. Model parameters and simulation conditions

Description	Symbol	Value (unit)
H_2 permeance	a_{H2}	1.6×10^{-10} mol/(m^2·s·Pa)
Selectivity, H_2/CO_2	$s_{H2/CO2}$	2.3
Selectivity, H_2/CH_4	$s_{H2/CH4}$	30
Selectivity, H_2/CO	$s_{H2/CO}$	24
Mass transfer coefficient	k	1×10^{-4}
Module diameter	D_{md}	0.1 m
Fibre outer diameter	D_o	250×10^{-6} m
Fibre inner diameter	D_i	200×10^{-6} m
Fibre length	L	0.6 m
Number of fibres	N_f	60,000
Feed temperature	T	313.15 K
Feed pressure	$P_{f,0}$	20×10^5 Pa
Feed molar flowrate	$F_{f,0}$	0.03, 0.015, 0.0075 mol/s
Feed composition, H_2	$x_{H2,0}$	0.75
Feed composition, CO_2	$x_{CO2,0}$	0.20
Feed composition, CH_4	$x_{CH4,0}$	0.04
Flow patterns	Feed-shell, counter-current flow	

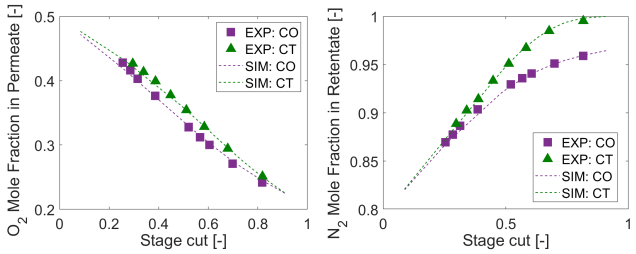

(a) (b)

Fig. 2. Comparison of model calculations and experimental data. (a) O_2 molar fraction in the permeate with respect to stage cut and (b) N_2 molar fraction in the retentate with respect to stage cut (= the total amount of permeate to feed). CO and CT represent co-current and counter-current, respectively.

3. RESULTS AND DISCUSSION

3.1 Model Validation

The developed mathematical model is validated against experimental data available in the literature (Feng et al., 1999), where air separation for producing pure nitrogen (N_2) and oxygen (O_2) was tested. The hollow fibre membrane module used in their study contained a bundle of 368 fibres with a length of 25 cm and an outer fibre diameter of 160 μm. The experiments were carried out in both the co- and counter-current flows without sweep gas. Feed air contains 20.5 vol% of O_2 and its balance N_2 at 690 kPa. Permeance parameters for O_2 and N_2 were reported to be 9.30 and 1.80 GPU, respectively (Gilassi et al., 2018).

Fig 2 presents model calculations and experimental data for the feed-shell operation. Calculated O_2 molar fraction in the permeate and N_2 molar fraction in the retentate are compared with their counterpart measurements under various feed flowrates that lead to a wide range of stage cut (= the amount of permeate to feed). As can be seen in Fig 2, the model calculations show excellent agreement with the experimental data both operations at a maximum relative error of 1.9% (for O_2 at the lowest stage cut for the co-current arrangement).

3.2 Simulation Results

Simulations for a single hollow fibre module are undertaken under three different feed flowrates using the model parameters and module specifications listed in Table 1. Fig 3 displays simulation results of axial variations in fluxes, flowrates, mole fractions and pressure drops in the feed and permeate sides at $F_{f,0} = 0.015$ mol/s. As can be seen in Fig 3a, permeate fluxes are maintained to be relatively constant throughout the membrane fibres. Interestingly, an H_2 flux decreases toward the exit of the feed channel while other components exhibit the opposite behaviour. This is attributed to the H_2 selective nature of the membrane used for simulation. Patterns of the resultant molar fractions shown in Fig 3c resemble those of the permeate fluxes. Normalised flowrates with respect to the inlet feed flowrates and outlet permeate flowrates for each component are displayed in Fig 3b. The outlet permeate flowrates are 6.0×10^{-3}, 8.7×10^{-4}, 1.6×10^{-5} and 5.0×10^{-6} mol/s for H_2, CO_2, CH_4 and CO, respectively. A decrease in the levels of CH_4 and CO is not significant in the feed stream, unlike H_2 and CO_2. Also the difference in the normalised flowrates of CH_4 and CO is trivial due to their similar selectivities. Finally, pressure drops are presented in Fig 3d, which are calculated with respect to the inlet feed pressure and permeate pressure at the closed end; the permeate pressure at the exit ($z = 0$) is 1×10^5 Pa. In this scenario, the permeate pressure drop is much higher than the feed side. This is due to the small diameter of membrane fibres where the permeate stream flows, which result in high flow velocity and frictional loss. Table 2 summarises the simulation results, including predicted stage cuts, retentate mole fractions and permeate mole fractions for each component. The achieved stage cut increases as the feed flowrate decreases, albeit not linearly. Since H_2 permeates the membrane rapidly compared to other components, the permeate stream has higher H_2 purity

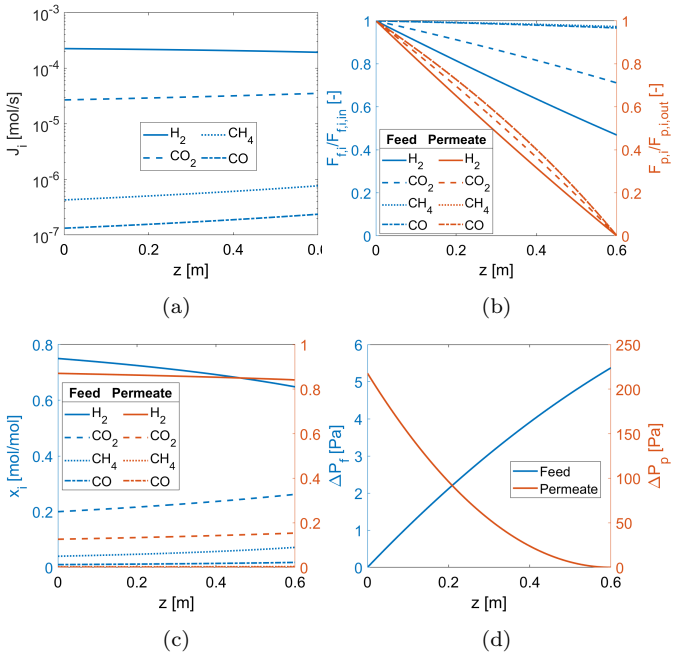

(a) (b) (c) (d)

Fig. 3. Simulation results of the representative scenario at $F_{f,0} = 0.015$ mol/s. (a) Axial variations of gas permeation fluxes, (b) normalised molar flowrates of each gas component in the feed and permeate sides, (c) molar fractions of each gas component in the feed and permeate sides and (d) pressure drops in the feed and permeate sides, i.e., $\Delta P_f = P_{f,0} - P_f$ and $\Delta P_p = P_{p,closed} - P_p$, where $P_{p,closed}$ is the permeate pressure at the closed end.

Table 2. A summary of simulation results

		Feed flowrate, $F_{f,0}$		
		0.03 mol/s	0.015 mol/s	0.0075 mol/s
Stage cut [%]		23.4	45.8	83.6
Retentate mol%	H_2	71.0	64.8	34.2
	CO_2	22.6	26.2	38.2
	CH_4	5.16	7.18	22.2
	CO	1.29	1.78	5.43
Permeate mol%	H_2	88.2	87.1	83.0
	CO_2	11.5	12.6	16.4
	CH_4	0.196	0.233	0.426
	CO	0.0606	0.0723	0.135

than the feed stream. Simulation results also demonstrate that the purity of H_2 in the permeate is lowered at a high stage cut, whereas the levels of other components become increased. Despite the elevated H_2 concentration in the permeate, it might not be sufficiently high for industrial applications. This implies that a multistage membrane configuration might be needed to meet quality standards. Conversely, CO_2, CH_4 and CO become concentrated in the retentate. When an H_2 selective membrane process is followed by syngas production, the separated CO_2 could be of low purity both in the retentate and permeate. This suggests that further CO_2 purification is required if the captured CO_2 is to be recycled and utilised elsewhere. Nonetheless, it should be mentioned that the aforementioned results are for a single module process with an H_2 selective membrane. The resultant concentrations of H_2 and CO_2 might vary significantly depending on the type of membranes, process design and operating conditions, which is addressed later.

3.3 Parametric Simulation Results

Figs 4, 5 and 6 present simulation results under a wide range of permeance, selectivity and mass transfer coefficient. The range of parameter values is chosen based on the literature (Scholes et al., 2010; Adhikari and Fernando, 2006; Lu et al., 2007).

First of all, the effects of a_{H2} and $s_{H2/CO2}$ on a stage cut and H_2 and CO_2 purities in the retentate and permeate are analysed, shown in Fig 4. $s_{H2/CH4}$, $s_{H2/CO}$ and k are kept to be constant at high values. For the simulated conditions, achieved stage cuts range between 2.0 and 83 %, highly affected by H_2 permeance. It can be seen that a high purity of H_2 in the permeate over 99% can be achieved at high a_{H2} and $s_{H2/CO2}$. Patterns of CO_2 purity in the permeate shown in Fig 4c are similar to those of H_2, with an inverted distribution. In the retentate, CO_2 becomes concentrated to 20 to 53 mol% depending on the membrane properties. An interesting finding is that gas purities in the permeate seem to be more influenced by $s_{H2/CO2}$, while those in the retentate appears to be more sensitive to a change in a_{H2}.

Fig 5 show simulation results for a CO_2 selective membrane with varied a_{CO2} and $s_{CO2/H2}$ at the fixed $s_{CO2/CH4}$, $s_{CO2/CO}$ and k. Stage cuts are predicted to be between 13 and over 99% for the simulated conditions. The predicted patterns are significantly different from those for an H_2 selective membrane; A higher purity of H_2 than its feed concentration is obtained in the retentate, achieving up to 91%, although an extremely low H_2 concentration in the retentate is observed at low $s_{CO2/H2}$ and high a_{CO2}, as in Fig 5d. This is because in such conditions the amount of both CO_2 and H_2 permeating through the membrane is substantial, which leads to concentrated CH_4 and CO in the retentate. On the other hand, CO_2 is concentrated to 20 to 70 mol% in the permeate stream. This suggests that it would be possible to accomplish over 90% purity of CO_2 if membrane and process designs are adequately selected.

Finally, a_{H2} and k are simultaneously varied while all selectivity parameters are fixed to 100. It appears from Fig 6a that a stage cut is more sensitive to a_{H2} than k at low a_{H2}, whereas the impact of k becomes more pronounced at high a_{H2}. Similar distributions can be found for H_2 and CO_2 concentrations in the retentate. As gas permeance increases, concentration polarisation becomes aggravated, which results in declined permeate flux. Therefore for a high permeance membrane, it is important to carefully select membrane modules and operating conditions for enhanced mass transfer. Since the selectivity parameters are chosen to be high for all components, over 96% purity of H_2 in the permeate can be achieved for all simulated ranges. The effects of concentration polarisation can be seen more clearly in Figs 6b and 6c; when mass transfer is poor, i.e., $k = 1 \times 10^{-7}$ m/s, H_2 purity in the permeate ranges between 99.6 and 96.5% for low permeance and high permeance membranes, respectively. However, at high k, $k = 1 \times 10^{-3}$ m/s, the discrepancy is almost negligible at 99.6 and 99.2% for low permeance and high permeance, respectively. Nonetheless, the influence of k on separation efficiency is believed to be less marked than permeance and selectivity parameters.

4. CONCLUSIONS AND FUTURE WORK

A number of computational simulations are performed using the reliable mathematical model developed in this work in order to investigate the effects of membrane properties and feed flowrates on H_2 and CO_2 separation efficiency after syngas production for the purpose of blue hydrogen. In the future, a detailed sensitivity study will be carried out for a multistage membrane gas separation process to identify critical design and operation parameters. Model-based optimisation will be followed to find the optimal process design and operation strategy for improved separation performance and reduced cost.

ACKNOWLEDGEMENTS

This work is supported by the National Research Foundation of Korea (NRF) grant funded by the Korea government (MSIT) (No. 2021R1C1C1006287).

REFERENCES

Adhikari, S. and Fernando, S. (2006). Hydrogen membrane separation techniques. *Industrial and Engineering Chemistry Research*, 45(3), 875–881.

Antonini, C., Treyer, K., Streb, A., van der Spek, M., Bauer, C., and Mazzotti, M. (2020). Hydrogen production from natural gas and biomethane with carbon capture and storage - A techno-environmental analysis. *Sustainable Energy and Fuels*, 4(6), 2967–2986.

Chu, Y., Lindbråthen, A., Lei, L., He, X., and Hillestad, M. (2019). Mathematical modeling and process parametric study of CO2 removal from natural gas by hollow fiber membranes. *Chemical Engineering Research and Design*, 148, 45–55.

Feng, X., Ivory, J., and Rajan, V.S. (1999). Air separation by integrally asymmetric hollow-fiber membranes. *AIChE Journal*, 45(10), 2142–2152.

Gilassi, S., Taghavi, S.M., Rodrigue, D., and Kaliaguine, S. (2018). Simulation of gas separation using partial element stage cut modeling of hollow fiber membrane modules. *AIChE Journal*, 64(5), 1766–1777.

He, G., Mi, Y., Lock Yue, P., and Chen, G. (1999). Theoretical study on concentration polarization in gas separation membrane processes. *Journal of Membrane Science*, 153(2), 243–258.

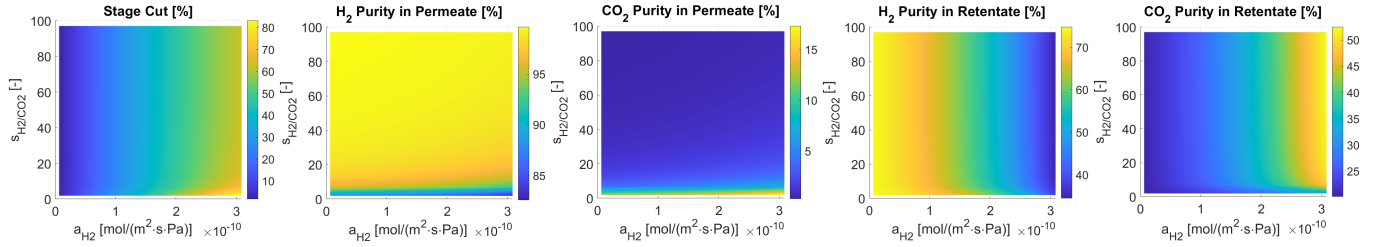

(a) (b) (c) (d) (e)

Fig. 4. Simulation results a H_2 selective membrane module by varying a_{H2} ($= 6.7\times10^{-12}$ to 3.35×10^{-10} mol/(m^2·s·Pa)) and $s_{H2/CO2}$ ($= 2$ to 100) at $s_{H2/CH4} = 100$, $s_{H2/CO} = 100$ and $k = 1\times10^{-4}$ m/s.

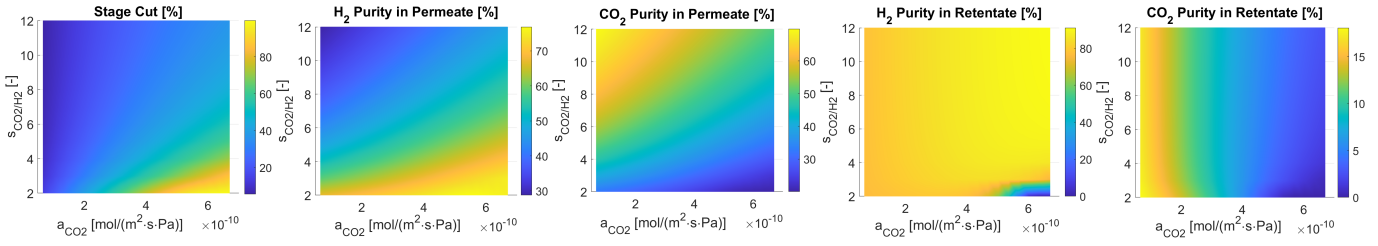

(a) (b) (c) (d) (e)

Fig. 5. Simulation results a CO_2 selective membrane module by varying a_{CO2} ($= 6.7\times10^{-11}$ to 6.7×10^{-10} mol/(m^2·s·Pa)) and $s_{CO2/H2}$ ($= 2$ to 12) at $s_{CO2/CH4} = 100$, $s_{CO2/CO} = 100$ and $k = 1\times10^{-4}$ m/s.

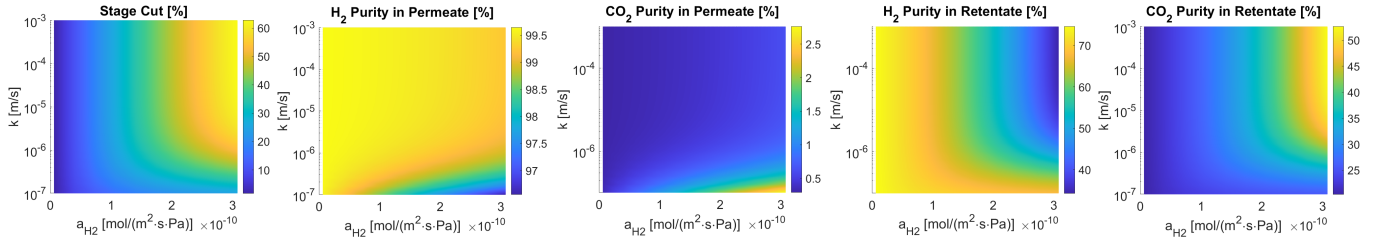

(a) (b) (c) (d) (e)

Fig. 6. Simulation results for a H_2 selective membrane module by varying a_{H2} ($= 6.7\times10^{-12}$ to 3.35×10^{-10} mol/(m^2·s·Pa)) and k ($= 1\times10^{-7}$ to 1×10^{-3} m/s) at $s_{H2/CO4} = 100$, $s_{H2/CH4} = 100$ and $s_{H2/CO} = 100$.

Khalilpour, R., Mumford, K., Zhai, H., Abbas, A., Stevens, G., and Rubin, E.S. (2015). Membrane-based carbon capture from flue gas: A review. *Journal of Cleaner Production*, 103, 286–300.

Lu, G.Q., Diniz da Costa, J.C., Duke, M., Giessler, S., Socolow, R., Williams, R.H., and Kreutz, T. (2007). Inorganic membranes for hydrogen production and purification: A critical review and perspective. *Journal of Colloid and Interface Science*, 314(2), 589–603.

Nagy, E., Nagy, R.R., Dudas, J., and Festschrift, E.D. (2013). Separate Expression of Polarization Modulus and Enrichment by Mass Transport Parameters for Membrane Gas Separation. *Ind. Eng. Chem. Res*, 52.

Ockwig, N.W. and Nenoff, T.M. (2007). Membranes for hydrogen separation. *Chemical Reviews*, 107(10), 4078–4110.

Scholes, C.A., Smith, K.H., Kentish, S.E., and Stevens, G.W. (2010). CO2 capture from pre-combustion processes—Strategies for membrane gas separation. *International Journal of Greenhouse Gas Control*, 4(5), 739–755.

Siagian, U.W., Raksajati, A., Himma, N.F., Khoiruddin, K., and Wenten, I.G. (2019). Membrane-based carbon capture technologies: Membrane gas separation vs. membrane contactor. *Journal of Natural Gas Science and Engineering*, 67(April), 172–195.

Voldsund, M., Jordal, K., and Anantharaman, R. (2016). Hydrogen production with CO2 capture. *International Journal of Hydrogen Energy*, 41(9), 4969–4992.

Wang, M., Lawal, A., Stephenson, P., Sidders, J., and Ramshaw, C. (2011). Post-combustion CO2 capture with chemical absorption: A state-of-the-art review. *Chemical Engineering Research and Design*, 89(9), 1609–1624.

Wang, R., Liu, S.L., Lin, T.T., and Chung, T.S. (2002). Characterization of hollow fiber membranes in a permeator using binary gas mixtures. *Chemical Engineering Science*, 57(6), 967–976.

Xu, J., Wang, Z., Qiao, Z., Wu, H., Dong, S., Zhao, S., and Wang, J. (2019). Post-combustion CO2 capture with membrane process: Practical membrane performance and appropriate pressure. *Journal of Membrane Science*, 581(November 2018), 195–213.

Zhang, Z., Wang, T., Blunt, M.J., Anthony, E.J., Park, A.H.A., Hughes, R.W., Webley, P.A., and Yan, J. (2020). Advances in carbon capture, utilization and storage. *Applied Energy*, 278, 115627.